Results in Physics 52 (2023) 106916

Contents lists available at ScienceDirect

Results in Physics

journal homepage: www.elsevier.com/locate/rinp

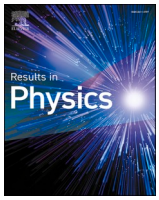

Modulating electronic properties of β-Ga_2O_3 by strain engineering

Ruijia Zhang [a,b,1], Min Li [b,1], Gai Wu [a,b,d], Lijie Li [c], Zhaofu Zhang [a], Kang Liang [a,b,d,*], Wei Shen [a,b,d,e,*]

[a] The Institute of Technological Sciences, Wuhan University, Wuhan 430074, China
[b] School of Power and Mechanical Engineering, Wuhan University, Wuhan 430072, China
[c] College of Engineering, Swansea University, Swansea SA1 8EN, UK
[d] Research Institute of Wuhan University in Shenzhen, Shenzhen 518057, China
[e] Hubei Key Laboratory of Electronic Manufacturing and Packaging Integration, Wuhan University, Wuhan 430072, China

ARTICLE INFO

Keywords:
β-Ga_2O_3
Strain engineering
Bandgap
Electron effective mass

ABSTRACT

β-Ga_2O_3 is a promising material for the development of next-generation power electronic and optoelectronic devices due to its exceptional properties, including ultrawide bandgap and thermodynamic stability. Strain engineering has emerged as a powerful method to modulate the physical properties of materials and has been widely employed in semiconductor devices to enhance their performance and functionality. Our study focuses on the effects of strain engineering on the electronic properties of β-Ga_2O_3. Using density functional theory, we calculated the band structures and electron effective masses of β-Ga_2O_3 under different strain states. Our investigation revealed that strain manipulation can induce an indirect-direct bandgap transition. Strain can also lead to changes in effective masses and anisotropy of electron mobility. Our calculations provide important insights into the potential of strain engineering as a powerful tool for modulating the electronic properties of β-Ga_2O_3, with important implications for practical device applications.

Introduction

Gallium oxide (Ga_2O_3) is one of the ultra-wide bandgap semiconductor materials with excellent material properties that have been extensively studied for its potential in various fields, including solar-blind UV photodetectors, gas sensors, photocatalysts, light-emitting diodes, and high-power electronic devices [1–11]. Its wide bandgap makes it suitable for high-voltage applications [12], and its high n-type conductivity and large optical bandgap make it a promising transparent conducting oxide for UV optoelectronic devices [13]. Among the six different polymorphs of Ga_2O_3, the monoclinic β phase is the most abundant and stable, owing to its exceptional chemical and thermal stability [14].

It is widely recognized that strain engineering is a powerful approach for modulating physical properties and enhancing the performance of electronic and photonic devices [15–23]. Strained silicon technology, in particular, has been extensively used in modern microelectronics, including CMOS devices, optoelectronic devices, sensors, and logic devices [24]. Considering that Young's modulus of β-Ga_2O_3 (150–190 GPa) is close to Young's modulus of silicon (130–190 GPa) [25,26], strain engineering is also potentially feasible in the electronic property modulation of β-Ga_2O_3. Currently, strain engineering has been widely applied to Ga_2O_3 and Ga_2O_3-based materials. Theoretical predictions of the bandgap tunability of α-Ga_2O_3 by hydrostatic, uniaxial, and equibiaxial strains have been reported by Ref. [27]. Calculations for the effects of uniform and epitaxial strain on the band structure of κ-Ga_2O_3 are also illustrated [28]. However, limited experimental studies have explored the strain effects on bulk β-Ga_2O_3. One recent study examined the effects of hydrostatic strain on the electronic properties (such as band structure, carrier effective mass and carrier mobility) of β-Ga_2O_3, revealing its band gap modulation, phase transition behavior, and anisotropic characteristics [29]. Another experimental study demonstrated the modification of the bandgap in β-Ga_2O_3 sheet through elastic strain using a modified bending method [30]. These results demonstrate the promising potential of strain engineering as an effective approach to enhance the performance of β-Ga_2O_3-based devices.

Based on the aforementioned research, it is suggested that strain can modify the bandgap of β-Ga_2O_3, leading to changes in its physical

* Corresponding authors at: The Institute of Technological Sciences, Wuhan University, Wuhan 430074, China.
E-mail addresses: liangkang@whu.edu.cn (K. Liang), wei_shen_@whu.edu.cn (W. Shen).
[1] Ruijia Zhang and Min Li contributed equally to this work.

https://doi.org/10.1016/j.rinp.2023.106916
Received 13 June 2023; Received in revised form 14 August 2023; Accepted 28 August 2023
Available online 29 August 2023

properties. It is worth noting that β-Ga_2O_3 is an indirect-bandgap material [31], which can limit its light emission efficiency. Additionally, the n-type conductivity of β-Ga_2O_3 is comparatively lower than other semiconductor materials such as SiC and GaN, which can reduce device performance [32]. Therefore, achieving a direct bandgap of β-Ga_2O_3 and studying the impact of strain on the electron effective mass is crucial, as this property can affect the material's electron conductivity, ultimately influencing device performance. In our study, we specifically investigated the impact of different types of strain (uniaxial, biaxial, and isotropic) on the structural parameters, bandgap structure, and electron effective mass of β-Ga_2O_3. While the aforementioned study primarily focused on hydrostatic strain [29], which is a more reasonable choice compared to isotropic strain, they did not consider uniaxial and biaxial strain. In contrast, our study innovatively incorporated these strain types, which are easier to apply in practical applications such as epitaxial growth. The results of our calculations will be valuable for fully realizing the potential of strain-engineered β-Ga_2O_3 in power electronics and optical applications.

Method

The structure and electronic properties of β-Ga_2O_3 are calculated using the first-principles plane-wave pseudo-potential method based on density functional theory (DFT). All calculations are carried out by PWmat, a GPU-based plane-wave pseudopotential code for DFT simulations [33]. The exchange–correlation potential is employed through the generalized gradient approximation (GGA) within the Perdew-Burke-Ernzerhof (PBE) function [34] and Optimized Norm-Conserving·Vanderbilt pseudopotentials [35]. Plane-wave cut-off energy of 70 Ry have been used for all structures. Before property calculations, geometry optimization is required to be converged. The number of Monkhorst-Pack k-point sampling [36] in the Brillouin zone is $2 \times 9 \times 5$ for the structural relaxation of the conventional cell containing 20 atoms. Subsequently, the optimized cell structure is transformed into a primitive unit cell containing 10 atoms for saving calculation time. In the self-consistent field (SCF) and density of states (DOS) calculations, the kmesh-resolved value is set at the same accuracy level of 0.035 (in the unit of $2\pi/$Å) using VASPKIT [37]. The convergence accuracy of total energy and force are 0.005 eV/atom and 0.005 eV/Å, respectively. The strain dependence of effective masses in the main CB valleys is evaluated. The carrier effective masses (m^*) is shown in Eq. (1)

$$\frac{1}{m^*} = \frac{1}{\hbar^2}\frac{\partial^2 E}{\partial k^2} \tag{1}$$

where m^* is the effective mass, $\hbar$ is the reduced Planck constant, E indicates the energy, and k is the wave vector in the reciprocal lattice. The values of m^* are obtained by fitting the energy dispersion of conduction band minimum to a parabolic function along different k directions in the vicinity of Γ. For the sake of higher accuracy and computational feasibility, the GGA + U method is adopted (see the Supplementary material for more details).

Fig. 1(a) shows the conventional unit cell and polyhedra of β-Ga_2O_3. The lattice parameters of the conventional cell, a = 12.05 Å, b = 3.00 Å, c = 5.74 Å, and $\beta = 103.55°$, are in good agreement with the previously reported values (a = 12.23 Å, b = 3.04 Å, c = 5.80 Å, and $\beta = 103.7°$) [38].There are two inequivalent Ga sites: Ga (I) and Ga (II). The Ga (I) atoms are bonded to four neighboring O atoms and the Ga (II) atoms are bonded to six neighboring O atoms. The calculated average bond lengths of Ga1-O and Ga2-O are 1.816 Å and 1.969 Å, respectively. Based on the calculated strain-free structure, the sizes of the strained lattice constants are determined. Three types of strain, uniaxial, biaxial, and isotropic strain with respect to three cell vectors a, b, and c are illustrated in Fig. 1 (b–d), where the directions of induced and optimized strain (ε_{ind} and ε_{opt}) are represented by arrows. The strains along the a-, b-, and c-axes are defined as $\varepsilon_a = (a - a_0)/a_0$, $\varepsilon_b = (b - b_0)/b_0$, and $\varepsilon_c = (c - c_0)/c_0$, where a_0, b_0 and c_0 are lattice constants at the strain-free state, respectively. Uniaxial strain is simulated by straining the lattice constant along b-axes while relaxing the other two constants. Biaxial strain is simulated by stretching the lattice constants along a- and c-axes

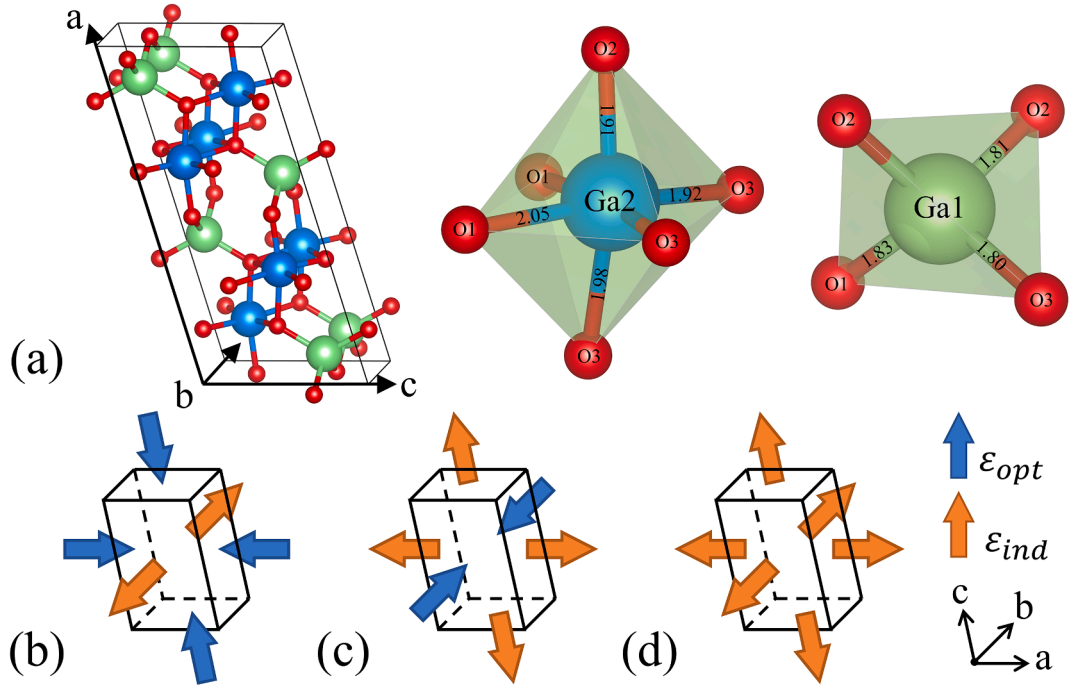

Fig. 1. (a) The conventional unit cell of β-Ga_2O_3 and the polyhedra of β-Ga_2O_3 with bond lengths and atom sites indicated. Schematic illustrations of (b) uniaxial (c) biaxial, and (d) isotropic strain models. The O atoms and two non-equivalent Ga atoms are distinguished by different colors. The orange and blue arrows represent induced strain (ε_{ind}) and optimized strain (ε_{opt}), respectively. (For interpretation of the references to colour in this figure legend, the reader is referred to the web version of this article.)

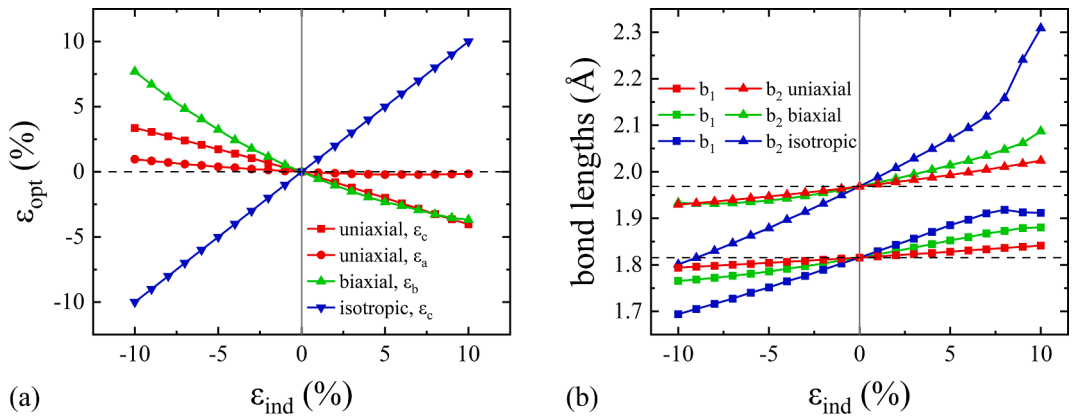

Fig. 2. (a) Optimized strain values and (b) bond lengths of β-Ga_2O_3 under different strain states: uniaxial, biaxial, and isotropic, which correspond to induced strain values.

simultaneously while relaxing that along *b*-axes. Isotropic strain is imposed by scaling all three lattice constants by the same factor. All calculations are carried out using 11 data points, covering a range of strain values from −10% to 10%, with a step of 1%.

Results and discussion

Lattice structure

The structure relaxation of strained β-Ga_2O_3 is performed firstly, and the results are shown in Fig. 2(a), which depicts the optimized changes in ε_a, ε_b, and ε_c as functions of the corresponding induced strain at each strain state.

In the application of uniaxial and biaxial strain models, the optimized strain is observed to decrease as the corresponding induced strain increases (see Fig. 2(a)). Of note is that the changes of optimized strain under uniaxial strain (ε_a and ε_c) are significantly smaller than that under biaxial strain (ε_b), with the biggest difference at –10% strain (ε_a = 3.36%, ε_c = 0.96% vs. ε_b = 7.70%). According to the Poisson effect, the optimized strain tends to change in the opposite trend of induced strain. Since the Poisson ratio of biaxially strained β-Ga_2O_3 is higher, it is reasonable that the changes in the structural parameters under biaxial strain are more pronounced. This phenomena has also been reported in the theoretical calculations concerning α-Ga_2O_3 [27] and κ-Ga_2O_3 [28].

Fig. 2(b) depicts lattice deformation, described by strain-induced bond length changes. As shown in Fig. 1(a), β-Ga_2O_3 has two inequivalent Ga sites and three inequivalent O sites, and the bond lengths between Ga1 (or Ga2) and the surrounding O atoms are close. Therefore, we calculated the average bond lengths of Ga1-O and Ga2-O, denoted as b1 and b2, respectively. It is found from Fig. 2(b) that the bond length variation between Ga1-O and Ga2-O are more or less proportional to induced strain in the investigated strain range, which indicates that there are no qualitative changes in the electronic structure of our relaxed strain model. These results further confirmed that our calculations are justified under the given conditions.

Table 1
The maximum and minimum bandgap values and the corresponding strain values at each strain state.

State	Maximum		Minimum	
	E_g/eV	ε_{ind}(%)	E_g/eV	ε_{ind}(%)
Uniaxial ($\boldsymbol{\varepsilon_{ind} = \varepsilon_b}$)	5.62	–9%	3.61	10%
Biaxial ($\boldsymbol{\varepsilon_{ind} = \varepsilon_{a,c}}$)	5.15	–4%	3.23	10%
Isotropic ($\boldsymbol{\varepsilon_{ind} = \varepsilon_{a,b,c}}$)	8.14	–10%	2.51	10%

Band structure

To have a complete image of the electronic band structure behavior under strains, the strain-induced changes on bandgaps are firstly determined. As given in the Supplementary material, the calculated band structure and DOS of unstrained β-Ga_2O_3 using GGA + U approach are represented in Fig. S1(a, b), yielding results close to other theoretical and experimental values [39–41]. Fig. 3(a–c) illustrates the strain

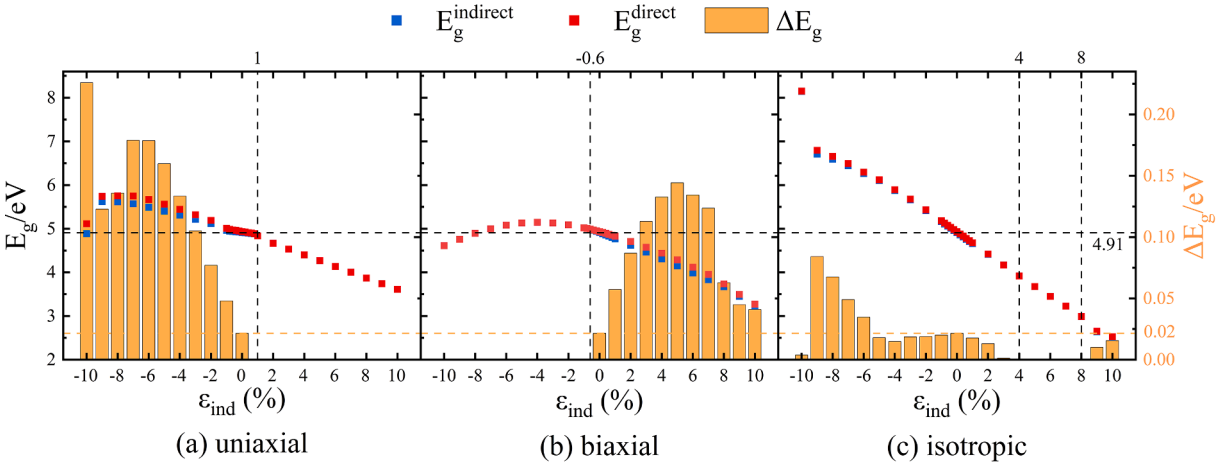

Fig. 3. Strain-induced effects on the bandgap of β-Ga_2O_3 as functions of (a) uniaxial, (b) biaxial, and (c) isotropic strain. The vertical lines indicate the strain point where indirect-to-direct transition occurs.

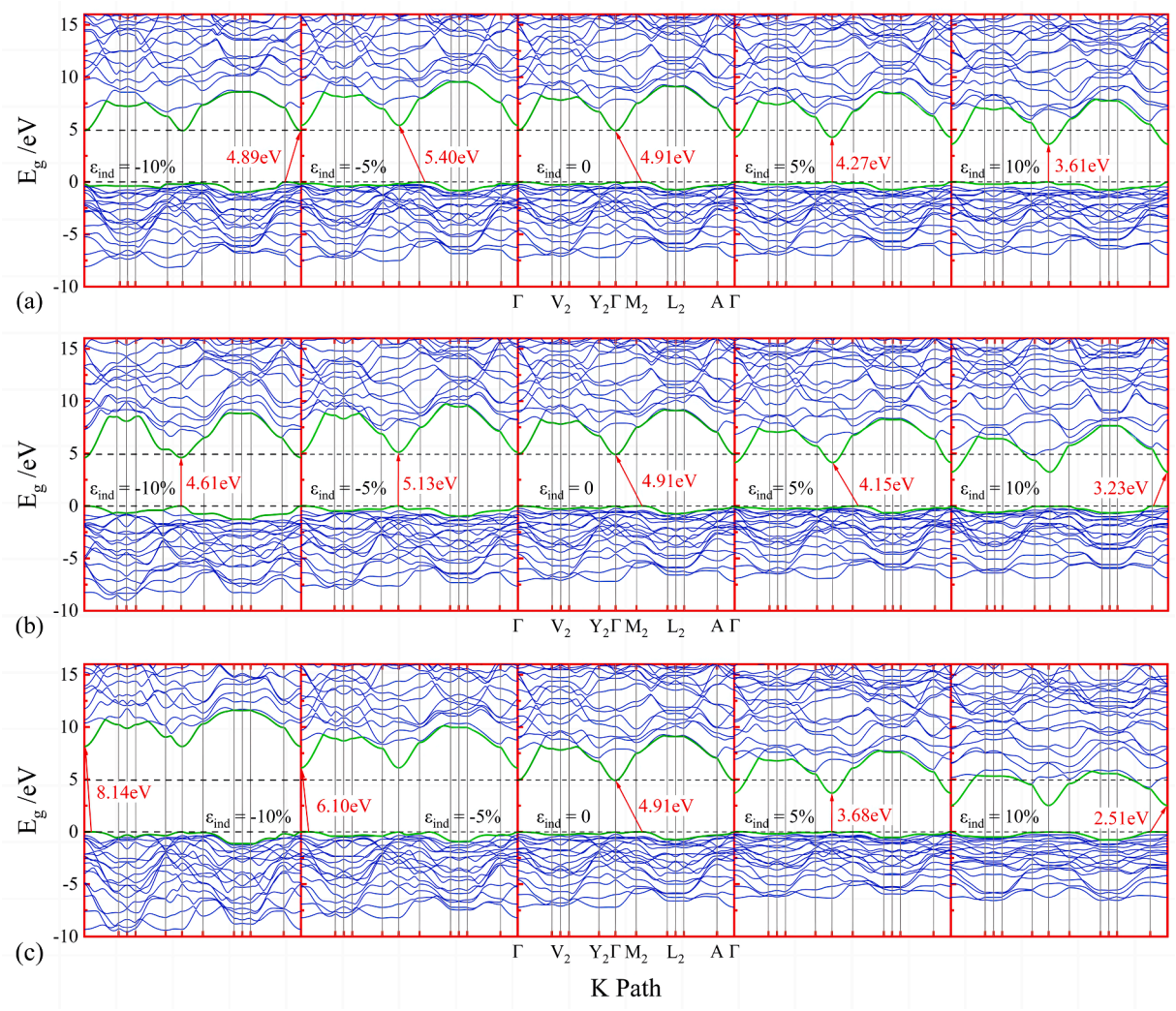

Fig. 4. Band structure evolution of β-Ga_2O_3 with respect to ±10% and ±5% (a) uniaxial, (b) biaxial, and (c) isotropic strain. The bandgap value of unstrained β-Ga_2O_3 (4.91 eV) is set as reference, the Fermi level is aligned to zero, and the arrows represent the directions from VBM to CBM.

Table 2
The average values of electron effective mass in β-Ga_2O_3 with different functionals, where m_0 is the free electron mass.

Functionals	m_e^*/m_0
GGA + U	0.353 (This work)
	0.22–0.28 [54]
GGA	0.12–0.13 [48]
LDA	0.23–0.24 [45]
Gau-PBE	0.22–0.30 [49]
HSE06	0.39 [52]
	0.28 [46]
B3LYP	0.34 [51]
Experiment	0.28 [40,50]

dependence of the direct bandgap E_g^{direct}, indirect bandgap $E_g^{indirect}$, and the energy difference ΔE_g ($\Delta E_g = E_g^{direct} - E_g^{indirect}$) for the three strain states: uniaxial, biaxial, and isotropic. The vertical lines indicate the strain point where indirect-to-direct bandgap transition occurs. Table 1 shows the list of maximum and minimum values of bandgap and the corresponding critical point under each strain state. It is known that achieving large strain in β-Ga_2O_3 can be challenging due to its relatively high elastic modulus and anisotropic monoclinic crystal structure [30]. Therefore, we conducted additional calculations for three different strain types within the range of −1% to 1%, with a step size of 0.2%. This finer approach enables a more detailed analysis of the strain-induced variations in bandgap and the transition from indirect to direct bandgap, as indicated in Fig. 3. The detailed figure, illustrating the comprehensive view of the bandgap variations within the −1% to 1% range, can be found in Fig. S2.

In the case of uniaxial or biaxial strain, the bandgap decreases as tension increases, while regarding compression, the bandgap slightly increases as compression increases within a certain range, and then begins to decrease with further compression, as indicated in Fig. 3(a, b). According to Table 1, the maximum bandgap value of 5.62 eV or 5.15 eV is achieved by applying compressive strain at −9% or −4%, respectively. On the other hand, the minimum bandgap value of 3.61 eV or 3.23 eV is observed under tensile strain at 10%. With regard to the isotropic strain, the bandgap evolution is almost linearly reduced as a function of strain (see Fig. 3(c)). The value of the bandgap decrease monotonously from 8.14 to 2.51 eV as the lattice strain increases within the investigated range. We note here that the change on the bandgap is significantly larger than that of uniaxial and biaxial strain, especially at −10% stain where drastic increasing of bandgap occurs, indicating the impact of isotropic change on the electronic property is stronger compared with the case of uniaxial and biaxial strain.

The underlying mechanism of bandgap evolution in β-Ga_2O_3 can be

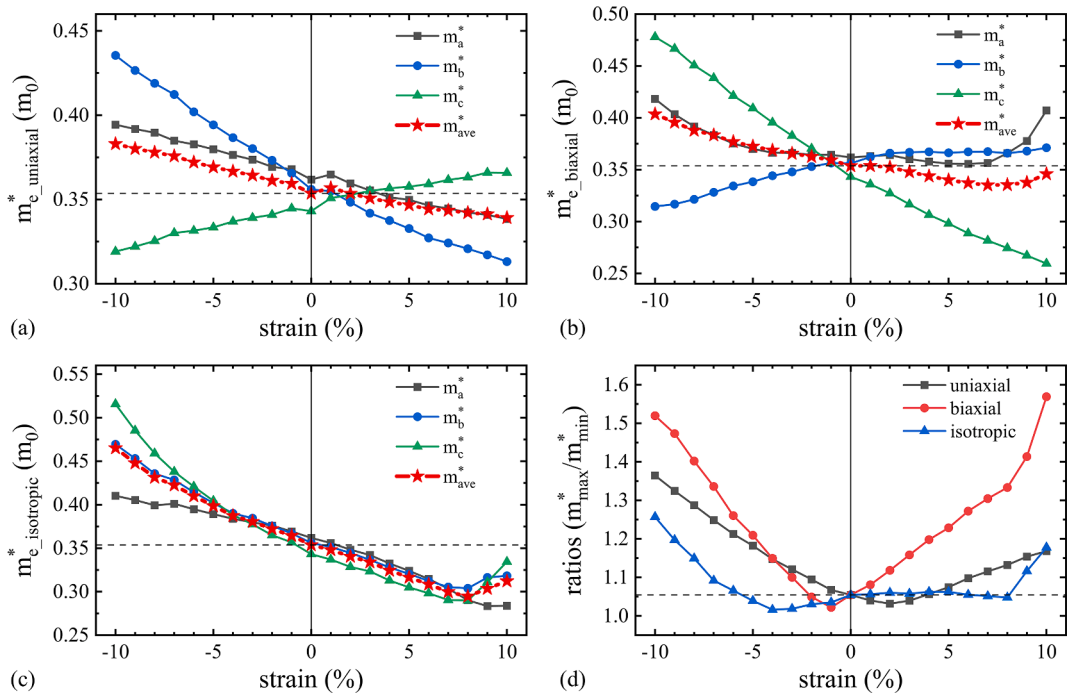

Fig. 5. Electron effective masses of β-Ga_2O_3 as functions of (a) uniaxial, (b) biaxial, and (c) isotropic strain and (d) changes on the electron effective mass ratio under each strain state. The dashed line represents the average electron effective mass and mass ratio of strain-free β-Ga_2O_3.

attributed to the strain-induced variations in the Ga-O bond length, which ultimately affect the distance between the conduction band and valence band. This phenomenon involves band repulsion, observed in various semiconductor and insulator materials [42,43], whereby the bandgap increases under compression and decreases under tension. However, when uniaxial or biaxial strain is applied, the light-hole (LH) band moves up under tensile strain, while the heavy-hole (HH) band moves up under compressive strain [15]. This leads to an inversion of the HH and LH bands at higher compression, resulting in a reduction of the bandgap with increasing compressive strain. This behavior has been reported in the literature for α-Ga_2O_3 [27] and κ-Ga_2O_3 [28] as well.

To understand the strain-induced changes in the bandgap characteristics in more detail, bandgap directness at each strain state is investigated, and the band structure of β-Ga_2O_3 at $\pm$10% and $\pm$5% strain is plotted in Fig. 4(a–c). The arrows represent the directions from VBM to CBM. Originally, the unstrained β-Ga_2O_3 features an indirect bandgap of 4.91 eV with the CBM at Γ point and the VBM at the Σ_{max} point along the M_2-D line, which corresponds to that reported in Ref. [44]. Of note is that the CBM remains at Γ point of the Brillouin zone in all cases. However, the VBM shifts to different k points due to strain-induced changes in lattice symmetry and Brillouin zone size, which ultimately affects the bandgap and band-edge properties.

From Fig. 3(a–c) and Fig. 4(a–c), the indirect-to-direct bandgap transition generally appears in uniaxial or isotropic tensile strain, as well as at biaxial compressive strain. As indicated in Fig. 4(a), when uniaxial compression is applied, the VBM remains at the Σ_{max} point along M_2-D line and changes to A point after exceeding $-$ 8% strain. While under tension, the VBM undergoes a shift from the Σ_{max} point to Γ point after exceeding 1% strain, resulting in a direct bandgap for β-Ga_2O_3. Similar parabolic variation characters are also observed in the case of isotropic strain, as displayed in Fig. 4(c). The VBM remains at the Σ_{max} point along M_2-D line and changes to Δ point, which is located near to the Γ point, for compressive strains exceeding $-$5%. When the tensile strain surpasses 4%, it becomes a direct-bandgap semiconductor. Of note is that, when the tensile strain exceeds 9%, the bandgap changes to indirect again with the VBM situated at A point. Intriguingly, for biaxial strain applied to β-Ga_2O_3, an opposite trend for the shift of bandgap directness is observed. The VBM remains at Σ_{max} point along M_2-D line and transitions to a point near the A point for tensile strains exceeding 8%. Conversely, for biaxial compressive strains greater than $-$0.6%, the VBM is located at the Γ point, as shown in Fig. 4(b).

When the strained β-Ga_2O_3 turns into a direct-bandgap semiconductor, it would exhibit a significant enhancement in its optical transitions around the fundamental adsorption edge, due to the elimination of phonon involvement to facilitate adsorption or emission. According to our results, the bandgap value of β-Ga_2O_3 can be modulated using strain engineering to exhibit better performance in power electronics and optical applications. Additionally, uniaxial or isotropic tensile strain and biaxial compressive strain can help to achieve direct gap material that benefits photon emission and absorption, indicating that bandgap tunning is manually feasible by introducing strain.

Electron effective mass

To further investigate the electron properties of β-Ga_2O_3, we calculated the effective mass under different strain states. Given the scarcity of p-type β-Ga_2O_3, we calculated the hole effective mass of β-Ga_2O_3, with the results detailed in the Supplementary material. However, due to the complex and highly anisotropic nature of hole effective mass and significant variations in previous results [45–47] for unstrained β-Ga_2O_3, establishing a clear relationship between hole effective mass and p-type conductivity remains challenging. Therefore, our study primarily focuses on electron effective mass. Specifically, we calculated the electron effective mass along three crystal directions ($\Gamma-Y_2$ [$-$1 1 0], $\Gamma-M_2$ [$-$1 1 1], and $\Gamma-$A [0 0 1]), denoted as m_a^*, m_b^*, m_c^* respectively. As presented in the Supplementary material, the electron effective mass of unstrained β-Ga_2O_3 is nearly isotropic. Reported results for the electron effective mass in β-Ga_2O_3 exhibit a wide range of values depending on different functionals and software methods [40,48–54,45,46], as shown in Table 2. Due to the differences in methodologies used in Functional analysis, there may be variations in band structure, such as the bandgap values. Thus, the determination of mass, relying on CBM, is prone to discrepancies resulting from variations in functional approaches. Additionally, although both our study and Ref. [54] employed GGA + U, it is important to note that differences in the assigned U values might

contribute to the divergent mass results obtained. Nonetheless, Our calculated average value of the electron effective mass in β-Ga_2O_3 (0.353 m_0) aligns consistently with several previous studies [51,52].

Next, we analyzed the dependence of electron effective mass of β-Ga_2O_3 on different strain states. The corresponding results are shown in Fig. 5(a–c). The strain-induced change on electron effective mass is discussed by considering the average value of the electron effective mass (m^*_{ave}) in the three directions. For qualitative investigation of anisotropy, the ratio of the maximum and minimum values (m^*_{max}/m^*_{min}) in m^*_a, m^*_b, m^*_c is introduced, as shown in Fig. 5(d). The values of m^*_{ave}/m_0 and m^*_{max}/m^*_{min} at different strain states are listed in Table S2.

A closer inspection of changes in the band structure with the increase in strain reveals that as the bandgap shrinks, the electron valleys at the CBM become increasingly "sharp" (see Fig. 4). In fact, from the $k{\cdot}p$ perturbation theory, electron effective mass (m^*_c) at the Γ point is approximately proportional to the bandgap value [55,56]. In each strain state, there is an almost linearly decreasing relationship between electron effective mass and strain, as shown in Fig. 5(a–c). We observed a modest decrease in m^*_{ave} with increasing isotropic strain (from 0.478 to 0.312), except for high applied tensile strain (>8%), while the variation of m^*_{ave} under biaxial strain exhibits a similar decreasing trend (from 0.450 to 0.346). When uniaxial strain is applied, a slight reduction (from 0.351 to 0.339) of the electron effective mass is also observed. From Fig. 5(d) and Table S2, we can arrive at a qualitative conclusion that the increasing uniaxial or biaxial strain at a critical point can cause the increasing mass ratios, while the anisotropy is found to be practically unchanged under isotropic strain (see Fig. 5(c)). Since the electron mobility $\mu = q\bar{\tau}/m^*_c$ is determined by electron effective mass, it is theoretically possible that the enhancement in the carrier mobility and electronic anisotropy can be achieved by increasing strain, with the correlated modulation on electron effective mass and mass ratios.

Conclusion

In summary, we have systematically studied the effect of strain on the crystal structure and electronic property of β-Ga_2O_3. It has been found that the bandgap monotonically decreases as the lattice constant increases in the isotropic strain case. However, in the case of uniaxial or biaxial strain, the bandgap decreases when the compressive strain exceeds a certain level. In most cases, for uniaxial or isotropic strain, β-Ga_2O_3 undergoes an indirect-to-direct bandgap transition under tensile strain and remains indirect for compressive strain, whereas for the biaxial strain, the shift of bandgap directness exhibits an almost opposite trend. Besides bandgap, our effective mass calculations show that the electron effective mass generally features a negative correlation with strain. Notably, the anisotropy of electron effective mass shows an upward trend in fluctuations under tension or compression. Our work can provide theoretical basis and experimental guidance for the development of β-Ga_2O_3-based devices by strain engineering.

CRediT authorship contribution statement

Ruijia Zhang: Investigation, Methodology, Writing – original draft. **Min Li:** Investigation, Methodology, Writing – original draft. **Gai Wu:** Resources, Software. **Lijie Li:** Writing – review & editing. **Zhaofu Zhang:** Formal analysis. **Kang Liang:** Investigation, Methodology, Writing – review & editing. **Wei Shen:** Conceptualization, Investigation, Methodology, Writing – review & editing, Resources, Software. **Ruijia Zhang** and **Min Li** contributed equally to this work.

Declaration of Competing Interest

The authors declare that they have no known competing financial interests or personal relationships that could have appeared to influence the work reported in this paper.

Data availability

Data will be made available on request.

Acknowledgements

This work is funded by the National Natural Science Foundation of China (Nos. 52202045, 62204173, 62004141), the Natural Science Foundation of Hubei Province (No. 2022CFB606), the Fundamental Research Funds for the Central Universities (Nos. 2042023kf0112, 2042022kf1028), the Guangdong Basic and Applied Basic Research Fund: Guangdong-Shenzhen Joint Fund (No. 2020B1515120005), the Guangdong Basic and Applied Basic Research Foundation (No. 2021A1515110890), Open Fund of Hubei Key Laboratory of Electronic Manufacturing and Packaging Integration (No. EMPI2023027), the Knowledge Innovation Program of Wuhan-Shuguang (Nos. 2023010201020255, 2023010201020243).

Appendix A. Supplementary data

See Supplementary material for the complete calculation details and results of strain-engineered β-Ga_2O_3. Supplementary data to this article can be found online at https://doi.org/10.1016/j.rinp.2023.106916.

References

[1] Higashiwaki M. β-Ga2O3 material properties, growth technologies, and devices: a review. AAPPS Bull 2022;32:3. https://doi.org/10.1007/s43673-021-00033-0.
[2] Wang Y, Su J, Lin Z, Zhang J, Chang J, Hao Y. Recent progress on the effects of impurities and defects on the properties of Ga_2O_3. J Mater Chem C 2022;10:13395–436. https://doi.org/10.1039/D2TC01128J.
[3] Meng L, Feng Z, Bhuiyan AFMAU, Zhao H. High-Mobility MOCVD β-Ga_2O_3 Epitaxy with Fast Growth Rate Using Trimethylgallium. Cryst Growth Des 2022;22:3896–904. https://doi.org/10.1021/acs.cgd.2c00290.
[4] Yuan Y, Hao W, Mu W, Wang Z, Chen X, Liu Q, et al. Toward emerging gallium oxide semiconductors: A roadmap. Fundam Res 2021;1:697–716. https://doi.org/10.1016/j.fmre.2021.11.002.
[5] Zhang H, Yuan L, Tang X, Hu J, Sun J, Zhang Y, et al. Progress of Ultra-Wide Bandgap Ga2O3 Semiconductor Materials in Power MOSFETs. IEEE Trans Power Electron 2020;35:5157–79. https://doi.org/10.1109/TPEL.2019.2946367.
[6] Hajime Asahi, Yoshiji Horikoshi, MBE Growth and Device Applications of Ga2O3, in: Molecular Beam Epitaxy: Materials and Applications for Electronics and Optoelectronics, Wiley, 2019: pp. 411–422. https://doi.org/10.1002/9781119354987.ch25.
[7] Guo R, Su J, Lin Z, Zhang J, Qin Y, Zhang J, et al. Understanding the Potential of 2D Ga_2O_3 in Flexible Optoelectronic Devices: Impact of Uniaxial Strain and Electric Field. Adv Theory Simul 2019;2:1900106. https://doi.org/10.1002/adts.201900106.
[8] Nakagomi S, Sakai T, Kikuchi K, Kokubun Y. β-Ga_2O_3/p-Type 4H-SiC Heterojunction Diodes and Applications to Deep-UV Photodiodes. Phys Status Solidi A 2019;216:1700796. https://doi.org/10.1002/pssa.201700796.
[9] Higashiwaki M, Jessen GH. Guest Editorial: The dawn of gallium oxide microelectronics. Appl Phys Lett 2018;112(6):060401. https://doi.org/10.1063/1.5017845.
[10] Higashiwaki M, Kuramata A, Murakami H, Kumagai Y. State-of-the-art technologies of gallium oxide (Ga2O3) power devices. J Phys D Appl Phys 2017;50. https://doi.org/10.1088/1361-6463/aa7aff.
[11] Kim M, Seo J-H, Singisetti U, Ma Z. Recent advances in free-standing single crystalline wide band-gap semiconductors and their applications: GaN, SiC, ZnO, β-Ga_2O_3, and diamond. J Mater Chem C 2017;5:8338–54. https://doi.org/10.1039/C7TC02221B.
[12] Higashiwaki M, Sasaki K, Murakami H, Kumagai Y, Koukitu A, Kuramata A, et al. Recent progress in Ga_2O_3 power devices. Semicond Sci Technol 2016;31(3):034001.
[13] Jaiswal P, Ul Muazzam U, Pratiyush AS, Mohan N, Raghavan S, Muralidharan R, et al. Microwave irradiation-assisted deposition of Ga_2O_3 on III-nitrides for deep-UV opto-electronics. Appl Phys Lett 2018;112(2):021105. https://doi.org/10.1063/1.5010683.
[14] von Wenckstern H. Group-III Sesquioxides: Growth Physical Properties and Devices. Adv Electron Mater 2017;3:1600350. https://doi.org/10.1002/aelm.201600350.
[15] Janik N, Scharoch P, Kudrawiec R. Towards band gap engineering via biaxial and axial strain in group IV crystals. Comput Mater Sci 2020;181:109729. https://doi.org/10.1016/j.commatsci.2020.109729.
[16] Qi Z, Sun H, Luo M, Jung Y, Nam D. Strained germanium nanowire optoelectronic devices for photonic-integrated circuits. J Phys Condens Matter 2018;30(33):334004.

[17] Attiaoui A, Moutanabbir O. Indirect-to-direct band gap transition in relaxed and strained Ge 1–x−ySixSny ternary alloys. J Appl Phys 2014;116(6):063712. https://doi.org/10.1063/1.4889926.

[18] Lee Y, Cho SB, Chung Y-C. Tunable Indirect to Direct Band Gap Transition of Monolayer Sc_2CO_2 by the Strain Effect. ACS Appl Mater Interfaces 2014;6:14724–8. https://doi.org/10.1021/am504233d.

[19] Desai SB, Seol G, Kang JS, Fang H, Battaglia C, Kapadia R, et al. Strain-Induced Indirect to Direct Bandgap Transition in Multilayer WSe_2. Nano Lett 2014;14:4592–7. https://doi.org/10.1021/nl501638a.

[20] Sakata K, Magyari-Köpe B, Gupta S, Nishi Y, Blom A, Deák P. The effects of uniaxial and biaxial strain on the electronic structure of germanium. Comput Mater Sci 2016;112:263–8. https://doi.org/10.1016/j.commatsci.2015.10.023.

[21] Tahini H, Chroneos A, Grimes RW, Schwingenschlögl U, Dimoulas A. Strain-induced changes to the electronic structure of germanium. J Phys Condens Matter 2012;24(19):195802.

[22] Zhou M, Liu Z, Wang Z, Bai Z, Feng Y, Lagally MG, et al. Strain-Engineered Surface Transport in Si(001): Complete Isolation of the Surface State via Tensile Strain. Phys Rev Lett 2013;111:246801. https://doi.org/10.1103/PhysRevLett.111.246801.

[23] Qin L, Duan Y, Shi H, Shi L, Tang G. Hybrid density functional theory studies of AlN and GaN under uniaxial strain. J Phys Condens Matter 2013;25(4):045801.

[24] H.H. Radamson, 3 - Strain engineering, in: H.H. Radamson, J. Luo, E. Simoen, C. Zhao (Eds.), CMOS Past, Present and Future, Woodhead Publishing, 2018: pp. 41–67. https://doi.org/10.1016/B978-0-08-102139-2.00003-3.

[25] Hopcroft MA, Nix WD, Kenny TW. What is the Young's Modulus of Silicon? J Microelectromech Syst 2010;19:229–38. https://doi.org/10.1109/JMEMS.2009.2039697.

[26] Luan S, Dong L, Jia R. Analysis of the structural, anisotropic elastic and electronic properties of β-Ga2O3 with various pressures. J Cryst Growth 2019;505:74–81. https://doi.org/10.1016/j.jcrysgro.2018.09.031.

[27] Kawamura T, Akiyama T. Bandgap engineering of α-Ga_2O_3 by hydrostatic, uniaxial, and equibiaxial strain. Jpn J Appl Phys 2022;61:021005. https://doi.org/10.35848/1347-4065/ac468f.

[28] Kim BG. Epitaxial strain effect on the band gap of a Ga2O3 wide bandgap material. J Korean Phys Soc 2021;79:946–52. https://doi.org/10.1007/s40042-021-00304-x.

[29] Zhang C, Wu X, Xing Y, Zhou L, Zhou H, Li S, et al. A first-principles study of hydrostatic strain engineering on the electronic properties of β-Ga2O3. Phys B Condens Matter 2023;660:414851. https://doi.org/10.1016/j.physb.2023.414851.

[30] Wang D, Lu X, Ding X, Zhao Y, Gou G, Shi Z, et al. Elastic strain modulation of energy bandgap in β-Ga2O3 sheet: Experimental and computational investigations. Mater Today Phys 2022;25:100697. https://doi.org/10.1016/j.mtphys.2022.100697.

[31] Liu X, Cheng K, Li R, Jia Y, Lu Q, Wang S, et al. Doping induced indirect-to-direct bandgap transition of two-dimensional Ga2O3. Appl Surf Sci 2021;553:149458. https://doi.org/10.1016/j.apsusc.2021.149458.

[32] W. Xu, Y. Zhang, Y. Hao, X. Wang, Y. Wang, T. You, X. Ou, G. Han, H. Hu, S. Zhang, F. Mu, T. Suga, First Demonstration of Waferscale Heterogeneous Integration of Ga_2O_3 MOSFETs on SiC and Si Substrates by Ion-Cutting Process, in: 2019 IEEE International Electron Devices Meeting (IEDM), IEEE, San Francisco, CA, USA, 2019: p. 12.5.1-12.5.4. https://doi.org/10.1109/IEDM19573.2019.8993501.

[33] Jia W, Cao Z, Wang L, Fu J, Chi X, Gao W, et al. The analysis of a plane wave pseudopotential density functional theory code on a GPU machine. Comput Phys Commun 2013;184:9–18. https://doi.org/10.1016/j.cpc.2012.08.002.

[34] Perdew JP, Kurth S, Zupan A, Blaha P. Accurate Density Functional with Correct Formal Properties: A Step Beyond the Generalized Gradient Approximation. Phys Rev Lett 1999;82:2544–7. https://doi.org/10.1103/PhysRevLett.82.2544.

[35] Hamann DR. Optimized norm-conserving Vanderbilt pseudopotentials. Phys Rev B 2013;88:085117. https://doi.org/10.1103/PhysRevB.88.085117.

[36] Monkhorst HJ, Pack JD. Special points for Brillouin-zone integrations. Phys Rev B 1976;13:5188–92. https://doi.org/10.1103/PhysRevB.13.5188.

[37] Wang V, Xu N, Liu J-C, Tang G, Geng W-T. VASPKIT: A user-friendly interface facilitating high-throughput computing and analysis using VASP code. Comput Phys Commun 2021;267:108033. https://doi.org/10.1016/j.cpc.2021.108033.

[38] Geller S. Crystal Structure of β-Ga2O3. J Chem Phys 1960;33(3):676–84.

[39] M. Orita, H. Ohta, M. Hirano, H. Hosono, Deep-ultraviolet transparent conductive -Ga2O3 thin films, 2014.

[40] Janowitz C, Scherer V, Mohamed M, Krapf A, Dwelk H, Manzke R, et al. Experimental electronic structure of In2O3 and Ga2O3. New J Phys 2011;13:085014. https://doi.org/10.1088/1367-2630/13/8/085014.

[41] Wei W, Qin Z, Fan S, Li Z, Shi K, Zhu Q, et al. Valence band offset of β-Ga2O3/wurtzite GaN heterostructure measured by X-ray photoelectron spectroscopy. Nanoscale Res Lett 2012;7:562. https://doi.org/10.1186/1556-276X-7-562.

[42] Y. Sun, S.E. Thompson, T. Nishida, Strain Effect in Semiconductors, Springer US, Boston, MA, 2010. https://doi.org/10.1007/978-1-4419-0552-9.

[43] Kim J, Fischetti MV. Electronic band structure calculations for biaxially strained Si, Ge, and III–V semiconductors. J Appl Phys 2010;108(1):013710. https://doi.org/10.1063/1.3437655.

[44] Peelaers H, Van de Walle CG. Brillouin zone and band structure of β-Ga_2O_3: Brillouin zone and band structure of β-Ga_2O_3. Phys Status Solidi B 2015;252:828–32. https://doi.org/10.1002/pssb.201451551.

[45] Yamaguchi K. First principles study on electronic structure of β-Ga2O3. Solid State Commun 2004;131:739–44. https://doi.org/10.1016/j.ssc.2004.07.030.

[46] Varley JB, Weber JR, Janotti A, Van de Walle CG. Oxygen vacancies and donor impurities in β-Ga2O3. Appl Phys Lett 2010;97(14):142106. https://doi.org/10.1063/1.3499306.

[47] Li L, Liao F, Hu X. The possibility of N-P codoping to realize P type β-Ga2O3. Superlattice Microst 2020;141:106502. https://doi.org/10.1016/j.spmi.2020.106502.

[48] He H, Blanco MA, Pandey R. Electronic and thermodynamic properties of β-Ga2O3. Appl Phys Lett 2006;88(26):261904. https://doi.org/10.1063/1.2218046.

[49] A. Mock, R. Korlacki, C. Briley, V. Darakchieva, B. Monemar, Y. Kumagai, K. Goto, M. Higashiwaki, M. Schubert, Band-to-band transitions, selection rules, effective mass and exciton binding energy parameters in monoclinic β-Ga2O3, (n.d.).

[50] Mohamed M, Unger I, Galazka Z, et al. The electronic structure of β-Ga2O3. Appl Phys Lett 2010;97(21):211903. https://doi.org/10.1063/1.3521255.

[51] He H, Orlando R, Blanco MA, Pandey R, Amzallag E, Baraille I, et al. First-principles study of the structural, electronic, and optical properties of Ga2O3 in its monoclinic and hexagonal phases. Phys Rev B 2006;74:195123. https://doi.org/10.1103/PhysRevB.74.195123.

[52] Ju M-G, Wang X, Liang W, Zhao Y, Li C. Tuning the energy band-gap of crystalline gallium oxide to enhance photocatalytic water splitting: mixed-phase junctions. J Mater Chem A 2014;2:17005–14. https://doi.org/10.1039/C4TA03193H.

[53] Ma N, Tanen N, Verma A, Guo Z, Luo T, Xing H (Grace), et al. Intrinsic electron mobility limits in β-Ga_2O_3. Appl Phys Lett 2016;109(21):212101. https://doi.org/10.1063/1.4968550.

[54] Zhang C, Liao F, Liang X, Gong H, Liu Q, Li L, et al. Electronic transport properties in metal doped beta-Ga2O3: A first principles study. Phys B Condens Matter 2019;562:124–30. https://doi.org/10.1016/j.physb.2019.03.004.

[55] Gupta S, Magyari-Köpe B, Nishi Y, Saraswat KC. Achieving direct band gap in germanium through integration of Sn alloying and external strain. J Appl Phys 2013;113(7):073707. https://doi.org/10.1063/1.4792649.

[56] David A, Miller B. Optical physics of quantum wells. In: Oppo G–L, Barnett SM, Riis E, Wilkinson M, editors. Quantum Dynamics of Simple Systems. 1st ed. CRC Press; 2020. p. 239–66. https://doi.org/10.1201/9781003072973-9.